Faster is Slower effect for evacuation processes: a granular standpoint

Bertrand Antti Maury, Etienne Pinsard, Sylvain Faure, Fatima Al Reda

Faster is Slower effect for evacuation processes: a granular standpoint

F. Al Reda[a], S. Faure[b], B. Maury[b,c], E. Pinsard[b,d]

[a] *Laboratoire Manceau de Mathématiques, Le Mans University, Le Mans, France*
[b] *Laboratoire de Mathématiques d'Orsay, Paris-Saclay University, CNRS, Orsay, France*
[c] *Département de Mathématiques et Applications, ENS PSL University, Paris, France*
[d] *Laboratoire Central de la Préfecture de Police de Paris (LCPP), Paris, France*

Abstract

The so-called Faster is Slower (FIS) effect is observed in some particular real-life or experimental situations. In the context of an evacuation process, it expresses that increasing the speed (or, more generally, the competitiveness) of individuals may induce a reduction of the flow through the exit door. We propose here a parameter-free model to reproduce and investigate this effect (more precisely its backward "Slower is Faster" equivalent). In spite of its non-smooth character, which makes it difficult to analyze, this granular approach is based on very basic ingredients in terms of behavior. In its native, purely asocial version, individuals are represented by hard-discs, each of which has a desired velocity, and the actual velocity is built as the projection of this field on the set of admissible velocities (which respect the non-overlapping constraints). We implement the *slower* effect by introducing here an extra step to account for the fact that individuals refrain from pushing, and therefore tend to reduce their desired velocity accounting for the velocities of people upfront. The present paper has two objectives: establish the relevance of this model by showing that it satisfactorily reproduces various empirical effects in highly crowded evacuations with various levels of competitiveness, and explore how it can be implemented to recover and explain the FIS effect. In this spirit, we confront this Inhibition-Based (IB) model to experimental data, focusing on the Faster is Slower effect. We show in particular that this approach makes it possible to accurately recover the effect of competitiveness upon power-law distributions of time lapses which have been experimentally observed. We also study the effect of mixed behaviors, by introducing a two-population model using both approaches. We

Preprint submitted to Elsevier

investigate in particular the effect upon evacuation efficiency of the ratio between competitive agents and non-competitive ones. In a similar context, we investigate the role of an obstacle placed upstream the exit upon evacuation efficiency.

Keywords: crowd motion, hard congestion, non-overlapping constraint, granular flows, evacuation scenarios, influence graphs, cone of vision.

---

1. Introduction

The Faster is Slower (FIS) effect pertains to a wide class of systems which may perform globally worse as their individual components strive to do better, or when an external forcing term is raised. Examples of such systems are given in Gershenson and Helbing (2015), in various contexts: vehicle or pedestrian traffic, ecology... Some simple mechanical systems with friction may also exhibit this sort of behavior: as detailed in Maury and Faure (2018), a mass pushed against and along an elastic wall with friction may undergo a reduction of speed, under some conditions, when the forcing term is increased. Let us also mention a real life phenomenon which exhibits this type of behavior (see de Gennes and Brochard-Wyart (2015), page 204): a viscous droplet hurtling down a slope under the action of its own weight, submitted to surface tension, is *slowed down* by an increase of gravity, because of the induced increase of the frictional contact zone.

In the context of crowd evacuation, this effect is commonly described as a decrease of the flow rate induced by an increase of desired velocities, driving forces, or eagerness to exit. It is qualified in Helbing et al. (2000) as one of the main characteristic features of escape panic. The authors show that in simulations, an increase of individual desired speed can lead to a lower exit speed in high congestion. While there is no consensus on the very cause of this effect, some models (like the Social Force model, or Cellular Automata) are able to reproduce it as soon as *friction* between individual is accounted for (see details below). We investigate in this paper the alternative possibility that the effect can be reproduced in a quantifiable way without any frictional ingredient, by means of a minimal model in terms of behavior, essentially parameter-less. As presented below, this minimal model will consist of an extension of an earlier granular model, introduced in Maury and Venel (2011), and used to model highly congested crowds. The term "granular" expresses that individuals are considered as hard spheres, and

the non-overlapping contraint is taken into account in a hard, nonsmooth way, whereas other strategies (like Helbing's Social Force Model) incorporate smooth repulsive forces to implement the tendency of individuals to stay away from each other. Note that this approach differs from standard mechanical model for granular flows (passive grains): it is first order in time, and friction is disregarded. This extension takes into account the effect of politeness at an individual level and can be used to model civilized evacuations. The granular nature of the model gives a robust way to treat contacts and overlappings without oscillations. We confront in the last part of our study our results to various experiments in the literature.

1.1. Experimental evidence

Experimental evidence of the FIS effect is reported in Garcimartín et al. (2014): the authors measured egress times for a population of 85 individuals under various conditions. A first set of experiments is carried out in a non-competitive spirit, and for the second set, the individuals are encouraged to "push and jostle for the exit within reason". Exit times in the second case are reported to be systematically larger than in the first situation, with an average increase of the order of 20 %.

Note that this effect strongly depends on the experimental setting. Some authors do not report any significant effect, see e.g. Daamen and Hoogendoorn (2012) where a large set of experimental data was collected to investigate the effect of various parameters upon the capacity of an exit door. In those experiments, no FIS effect was observed: the increase of stress level simply leads to higher speed and higher capacity. The same observation is made in Nicolas et al. (2017), where the effect of individual behavior upon the global flow though a narrow doorway is investigated. It is argued that the level of competitiveness is not large enough in their experiments to reproduce this effect. More generally in Haghani (2020) the author shows inconsistencies in experimental evidences of the FIS effect, which depends highly on structural or behavioral characteristics of the experiment. Similar conclusions are drawn in Feliciani et al. (2020), the effect can be observed in certain circumstances, but not systematically.

Since the effect is particularly significant for highly congested and aggressive crowd, such experiments are delicate to carry out in a controlled experimental setting, for obvious safety reasons. Some authors have investigated the possibility to reproduce this effect in animals. In this spirit (see Pastor et al. (2015)), some experiments have been performed on a herd of sheep

rushing through a door, craving for food. The level of competitiveness is monitored by the temperature, owing to the fact that the individual behavior of a sheep is strongly affected by thermal conditions. The time lapses between consecutive egresses of entities is observed to be significantly larger in the case with high competitiveness. The authors propose in the same paper a purely mechanical version of the experiment: The entities are rigid grains flowing through a bottleneck, and they investigate the dependence of the flow rate of grains upon the inclination angle of the setting. They observe the following effect: in the clogging regime, increasing the angle (and thus increasing the *driving force*) reduces the flow rate.

Effect of an obstacle

Let us also mention another effect, that is the fluidizing effect of an obstacle. Since the obstacle can be seen as a way to passively reduce the velocity of (some) individuals, the fact that it may increase the flow rate can be interpreted as a special instance of the FIS phenomenon (more precisely its equivalent reverse Slower is Faster). Even more than the plain FIS effect, this paradoxical effect is delicate to reproduce and observe for pedestrian crowds; for grains, the effect is fairly easy to observe.

The experimental setting described in Yanagisawa et al. (2009) is based on pedestrians going through a 50 cm exit. Two series of experiments are reported, a first one with no obstacle, and a second one with a cylindrical obstacle located upstream the exit, non symmetrically. A 4 % increase of the flux by addition of the obstacle is reported. This small increase is considered as statistically significant by the authors.

In Jiang et al. (2014), the effect of pillars placed upstream an exit of width 1 m is investigated, experimentally. The measured mean flux is about 16 % larger for the case with two obstacles ($2.9\,\mathrm{Ps}^{-1}$, i.e. 2.9 persons per second), compared to the situation with no obstacle ($2.5\,\mathrm{Ps}^{-1}$). Note that the number (three) of experimental runs for each case does not make it possible to give confidence intervals.

In Helbing et al. (2005), several experiments are presented. In particular, the authors consider the evacuation of a room in panic-like situation. Placing a board of width 45 cm upstream the exit (of width 82 cm, the distance to the exit is not given) is shown to reduce the evacuation time by 30 %.

More significant effects have been established for non-human entities. In Lin et al. (2017), experiments involving mice are described. Mice (crowd of 80 individuals were considered) are driven to pass through a narrow exit,

with or without obstacle. The presence of an obstacle is shown to reduce the evacuation time by a maximum of 36 % (the effect varies with the position of the obstacle). The maximal effect is obtained for an obstacle placed at 4 cm from the exit, while mice are typically 3 cm wide and 10 cm long.

The experiments proposed in Zuriguel et al. (2016) involve sheep. The authors investigate the effect of placing a cylindrical obstacle (with diameter 114 cm) upstream a 96 cm exit. Distances to the exit range from 60 cm to 1 m, while the width of a sheep is about 35 cm. They report a positive effect of the obstacles for distances of 80 and 100 cm (for 60 cm, the obstacle is counter-productive).

Recent experiments are also presented in Feliciani et al. (2020), with a circular obstacle. It is observed that an obstacle does not reduce the density, neither the level of compression but, in non-emergency evacuations, it forces the people to leave the exit in a more organized way.

This effect is still debated in the literature, as detailed in the recent review proposed in Shiwakoti et al. (2019).

1.2. Modeling aspects

Social force model

In its native form, this model consists in a set of second order in time equations of motions for each agent, obtained in analogy with Newton's second law. Various force terms encode repulsive or attractive interactions between individuals and their neighbours or nearby obstacles. A set of individual parameters for body mass, individual response time, compression and friction are required for this model. We refer to Corbetta et al. (2015) for a recent work dedicated to estimating those parameters from real-life experiments.

As illustrated by numerical tests (Helbing et al. (2000)), the FIS effect is reproduced by this model. The authors observe a decrease of 26.7 % in the average flow when the desired velocity undergoes an increase from $1.7\,\mathrm{m\,s^{-1}}$ to $3\,\mathrm{m\,s^{-1}}$. The possibility to recover this effect relies on a friction term that is added to the forcing term, and penalizes the relative velocity of people in contact. Increasing the desired velocity leads to smaller inter-individual distances, which yields stronger frictional effects. These frictional effects tend to freeze the congested crowd, which favors clogging, and reduces the overall flow rate. Statistical analysis in Cornes et al. (2021) on the congestion effects for the social force model shows the link between an increase in desired velocity and the formation of clusters. The stiffness parameter in the compression term is also shown in Sticco et al. (2020) to play a role in the FIS effect. Low

values of this parameter lead to additional sliding friction term that favors the formation of clogs in front of a door, as mentioned earlier. The flow decreasing percentage is also significant for some modified versions of the social force model described in Parisi and Dorso (2007) and Lakoba et al. (2005). A decreasing percentage of 35.4 % is found in Parisi and Dorso (2007) when the desired velocity increases from $1.38\,\mathrm{m\,s^{-1}}$ to $2.5\,\mathrm{m\,s^{-1}}$. In Lakoba et al. (2005), the authors observed the FIS effect for a higher increase in the desired velocity. Notably, the flow decreases by 30 % when the desired velocity passes from $1.5\,\mathrm{m\,s^{-1}}$ to $4.5\,\mathrm{m\,s^{-1}}$.

A large set of numerical experiments based on the same approach is described in Escobar and Rosa (2003). The authors investigate the effect of panic on the efficiency of room evacuation. The panic is again accounted for by increasing the desired velocity of individuals. It is observed that, for small crowds (i.e. under 100 individuals), panic tends to speed up the process, whereas for larger crowds, increasing some desired velocities may harm it. More precisely, when the fraction of "panicked" people exceeds a certain value, a decrease of the evacuation efficiency can be observed. In Ruifeng Cao et al. (2019), the authors reproduced the FIS effect by introducing a modified version of the original social force model based on developing a give-way behavior of evacuees. The desired velocity of a give-way individual decreases exponentially when other individuals approach his near surrounding. This behavior is shown to reduce the frequency of clogging, hence reducing the evacuation times.

Cellular automata

Cellular Automata (CA) are based on a cartesian grid, each cell of which is assumed to contain 0 or 1 individual (see Schadschneider (2001); Schadschneider and Seyfried (2009); Kirchner and Schadschneider (2002)). In the *parallel update* setting, the evolution model consists of a sequence of updates, where each particle-individual may change their position to a neighboring cell, or remain in the same cell. The transition probabilities between two updates are computed using a weight for each neighbouring cell. This weight depends on the so-called floor field, which encodes individual tendencies and is typically the distance to the exit. It is set to 0 for cells which are already occupied by someone.

Motions for all individuals are then drawn independently, according to these probabilities. This first step is likely to lead to *conflicts*, i.e. 2 or more individuals aim to occupy the same cell. In the basic version of the approach,

these conflicts are usually resolved by picking the individual which is the most committed (regarding their individual tendency to reach this cell).

Those models are also known to reproduce the FIS effect under some conditions. The crucial ingredient is again *friction*, but this notion takes a particular form in the context of CA methods. Friction is implemented by modifying the handling of conflicts, in the parallel update algorithm described above. Adding friction amounts to considering that there is a probability $\mu > 0$ that the conflict is resolved by leaving all competitors in their cells: nobody moves. Here lies the *Slower* feature. The *Faster* ingredient is implemented by considering that the parameter which conditions the transition probabilities (usually denoted by k_S) quantifies the eagerness of individuals to move forward. To sum up, the main parameters of this model are the space step size (which conditions in a rigid way the maximal density that is allowed), the parameter k_S which characterizes the relation between the so called floor field (typically the distance to the exit) and the transition probabilities, and the friction parameter μ.

Parameter studies proposed in Kirchner et al. (2003) exhibit a significant effect in terms of increase of the evacuation time. More precisely, when the friction parameter is set at a high value ($\mu = 0.9$), the minimal evacuation time is achieved for an intermediate desired speed, more precisely by an intermediate value of the parameter which converts the floor field into biased transition probabilities. An increase of this time by 50% is reported (Figure 8 of Kirchner et al. (2003)). Let us point out that, in the context of CA, the desired speed is actually limited by the ratio between the space step size and the time step. Having k_S increase from 0 corresponds at first to increasing the speed, but large values of k_S rather lead to favor the direction along the axes (vertical or horizontal) that reduces best the floor field. In other words, increasing k_S beyond some threshold value essentially amounts to change the expected direction of agents, and not their speed (see Figure 5.3 in Maury and Faure (2018) for an illustration of this effect). The effect of friction is clear (as detailed also in Maury and Faure (2018), Section 10.1): large values of k_S induce a systematic tendency to move forward, which increases the number of conflicts, thus slowing down the overall evacuation process by an increased probability of "do-nothing" events.

Large sets of numerical experiments based on CA are also presented in Xiaoping et al. (2010). The total evacuation time for 200 virtual individuals is computed for several desired speeds. The evacuation time is reduced by 40 % when the desired speed goes from $0.5\,\mathrm{m\,s^{-1}}$ to $1.5\,\mathrm{m\,s^{-1}}$. Note that this

time increases when the speed further increases.

Granular model

In a fully different setting, the granular approach (see Maury and Venel (2011)) is also able to recover this effect, whereas no friction is accounted for. In its basic version, this granular model (described in detail in Section 2) is based on the consideration that individuals are identified with fully asocial rigid discs which tend to achieve their own agenda (encoded is a desired velocity), disregarding neighbors. Interactions are induced by physical contacts between those grains, whenever the non-overlapping constraint is activated. The actual velocities of individuals are then computed as the projection of the desired velocity field on the set of admissible velocity fields (respecting the non-overlapping constraint between individuals in contact). This model was initially developed to handle collisions in the inertial setting, fluid-particle suspension (see Glowinski and Maury (1997)). Numerical simulations of the granular model are performed in Maury and Venel (2009) where the authors show the ability of the model to reproduce two crowd motion effects: lane formation in counter flowing crowd and the formation of arches in evacuation situations. The creation of jams is furthermore investigated in Faure and Maury (2015) and it is shown that static jams systematically occur when the width of the exit door is less than twice the people diameter. However, when the door width is greater than 2.7 the size of an individual such jams are actually rare. An extension of the model is also proposed in the same reference to account for the capacity of individuals to "take upon themselves" and stop pushing whenever it is obviously useless. It is shown that incorporating this individual tendency to *slow down* in some situations has the effect to *speed-up* the evacuation process.

As the previous ones, this approach relies on several tuneable parameters. The purpose of the present paper is to propose a parameter-free setting to reproduce and investigate the FIS phenomenon.

1.3. Principles of the present approach

We propose here a minimalist model to better understand the mechanisms of the Faster is Slower effect. Our starting point is the so-called granular model mentioned at the end of the last paragraph. This model (Maury and Venel (2011)) was inspired from contact models developed for handling collisions and possibly numerical overlapping in fluid particle simulation (see Glowinski and Maury (1997)). It is based on the following principles: N

individuals are identified to hard discs, and a collection of desired velocities is given. For a given configuration (with no overlapping, but possibly with contacts), we define the feasible set as the set of velocities that are admissible with respect to the non-overlapping constraint: for any two grains already in contact, the relative velocity is not allowed to further decrease the distance between centers. The actual velocity of the crowd is then simply defined as the projection (in a least-square sense) of the desired velocity field on the feasible set. This approach is natively parameter-free (if one considers that changing the speed of individuals amounts to make a change of variable in time). It is also very crude in terms of behavior, in the sense that the underlying behavior is purely *a*–social: all individuals tend to achieve their goals disregarding other people, and the interactions emerge as a consequence of the non-overlapping constraint. Therefore, the approach is fully *mechanical* in the sense that the Lagrange multipliers arising to implement the non-overlapping constraint can be interpreted as interaction forces, which naturally obey the Law of Action-Reaction (see next section for more details on those aspects).

We propose to incorporate the *Slower* feature (from the *Slower is Faster* effect) in the following way: we consider now that the individuals have the capacity and the tendency to account for the people they see (i.e. in front of them). Each pedestrian is assumed to adapt their desired velocity with respect to the velocities of the neighbors located in their cone of vision. More precisely, each individual picks the velocity that is the closest to their desired one, subject to the non-overlapping constraint with the people upfront, assuming that their velocities are known. If the situation is hierarchical (as will be detailed below, it corresponds to the situation where individuals can be indexed in a way which respects the oriented graph induced by the cones of vision), all velocities can be determined in a unique way, by starting with the people upfront who are not constrained, and then sweeping over the hierarchy. The obtained velocity field, which we shall call *adapted*, may not be feasible because some constraints may have been disregarded (typically in the case of two side-to-side pedestrians striving to reach the same point upfront, who experience a non-anticipated lateral collision).

From a modeling standpoint, the approach described above implements the following behavior: each individual inhibits their tendency to move forward by reducing their frontward velocity to avoid pushing on people in front of them. This approach therefore implements some sort of social behavior, which leads to *slower* individuals, without any tunable parameter. The core

of this paper consists in showing that this minimalist approach makes it possible to recover and quantify in different manners the effect, in comparison to a set of experiments in the literature studying the Faster-Is-Slower for pedestrians.

2. Model formulation

We consider N individuals, which we identify with discs centered at $q_1,\ldots,\ q_N$, with common radius r. The configuration at some instant is $q = (q_1, \ldots, q_N)$. We denote by U_i the desired velocity of individual i, i.e. the velocity they would like to have if they were alone. We shall assume in the sequence that $U_i = U(q_i)$, where $U(\cdot)$ is a common desired velocity field (individuals are interchangeable), but this assumption is not mandatory. In the following, U_i will stand for $U_i(q_i)$. We define the set of feasible configurations by:

$$K = \left\{ q \in \mathbb{R}^{2N}, \quad D_{ij}(q) \geq 0, \quad \forall i \neq j \right\} \tag{1}$$

where $D_{ij}(q) = |q_i - q_j| - 2r$ is the body distance between individuals i and j (see Figure 1). The non-overlapping constraint simply writes $q \in K$.

2.1. Plain granular model

We first describe the model proposed in Maury and Venel (2011), which handles individuals as fully asocial entities which tend to achieve their own goals. To any feasible configuration $q \in K$ one can associate a set of feasible velocities, i.e. velocities which do not lead to overlapping. More precisely

$$C_q = \left\{ w = (w_1, \ldots, w_N) \in \mathbb{R}^{2N}, \quad \forall i \neq j \quad D_{ij}(q) = 0 \Rightarrow e_{ij} \cdot (w_i - w_j) \leq 0 \right\}, \tag{2}$$

where $e_{ij} = (q_j - q_i)/|q_j - q_i|$ is the unit vector from i to j. The model simply expresses that the actual velocity $u = dq/dt$ is determined by

$$u = P_{C_q} U \tag{3}$$

where $U = (U_1, \ldots, U_N)$ is the collection of desired velocities, and P_{C_q} is the euclidean (least-square sense) projection on the feasible set C_q.

In spite of its formal simplicity, this model raises deep issues in terms of mathematical analysis: due to the hard-sphere setting, it does not fit in the

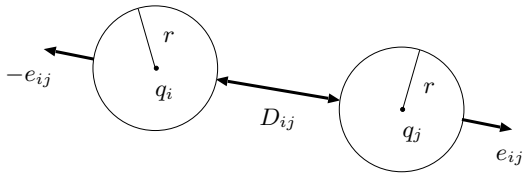

Figure 1: Notation

standard framework of smooth Ordinary Differential Equations. Based on tools from convex analysis, in particular pertaining to the so-called sweeping process (Moreau (1977)), existence and uniqueness of a solution can be established (see Maury and Venel (2011)). In its basic version, this model actually presents a very particular structure: under some conditions it can be interpreted as a *gradient flow* (i.e. an evolution along the steepest descent direction) for a certain dissatisfaction. More precisely, if one assumes that the desired velocity of an individual depends upon their position only, and that it writes as the negative gradient of a dissatisfaction function D (typically the distance to a commun target), i.e. if

$$U_i = -\nabla D(q_i), \tag{4}$$

then the model can be written

$$\frac{\mathrm{d}q}{\mathrm{d}t} \in -\partial\Psi(q), \text{ with } \Psi(q) = \sum_{i=1}^{N} D(q_i) + I_K(q), \tag{5}$$

where I_K denotes the so-called indicator function of the feasible set K (it vanishes in K, and takes the value $+\infty$ outside K), and $\partial\Psi$ denotes the *Fréchet subdifferential* of Ψ. We refer the reader to Maury and Venel (2011) for more details on this formalism, and we shall simply keep in mind that the evolution model, once the gradient flow structure is set, is entirely contained in this global dissatisfaction function which encodes both the individual tendencies (sum of the $D(q_i)$'s) and the non-overlapping constraint (indicator function I_K).

2.2. Inhibition-Based granular model

We propose to enrich the previous approach by incorporating an intermediary step to implement the tendency of people to refrain from pushing on people in front of them, whenever it is obviously useless. We shall restrict

ourselves here to cases which exhibit a strict hierarchy in terms of influence. More precisely, we introduce a so-called *influence graph* (which is likely to depend on the configuration). This object is a directed graph, the vertices of which are the individuals $1,\ 2, \dots, N$, and we shall consider that there is an arrow from i to j if i is influenced by j. In practical applications to evacuation processes, we shall consider that j influences i if j lies in the cone of vision of i (see Section 2.3). We denote by V_i the set of individuals that influence i. Now we make an essential assumption: the influence graph is supposed to be *acyclic*. It implies in particular that $j \in V_i \Longrightarrow i \notin V_j$, but it also excludes the presence of cycles of any length.

As we shall see in Section 2.3, this assumption makes sense in evacuation situations, when all individuals in each zone tend to reach the same exit. We refer to Remark 1 for some comments on the problem which is obtained when this assumption of hierarchical influence is ruled out. The influence graph being acyclic, it can be seen as a partial order, and the topological *sorting algorithm* makes it possible to build a total order compatible with the partial one. In other words, it is possible to re-index individuals in such a way that $j \in V_i$ implies $j > i$.

We propose now to define the inhibited desired velocities $\overline{U}_N$, $\overline{U}_{N-1}$, $\dots$, by initiating the downward induction by $\overline{U}_N = U_N$ (since N is influenced by nobody, they keep their desired velocity as if they were alone), and the next velocities $\overline{U}_{N-1}$, $\overline{U}_{N-2}$, $\dots$, by the following procedure:

$$\overline{U}_i = \underset{w \in C_i}{\operatorname{argmin}} \frac{1}{2}|w - U_i|^2, \quad \forall i = 1, \dots, N \tag{6}$$

where C_i is the set of feasible velocities for i, defined by

$$C_i = \left\{ w \in \mathbb{R}^2, \quad \forall j \in V_i, \quad D_{ij}(q) = 0 \Rightarrow e_{ij}(q) \cdot (w - \overline{U}_j) \leq 0 \right\}. \tag{7}$$

Note that this set only depends on the inhibited velocities of individuals j for $j > i$. Thanks to the hierarchy, these velocities have already been determined in the induction process, therefore $\overline{U}_i$ is uniquely determined as the minimizer of a quadratic functional over a well-determined set C_i, which is convex as an intersection of half spaces.

Projection step

Once the inhibited velocities have been determined, the obtained velocity field $\overline{U} = (\overline{U}_1, \dots, \overline{U}_N)$ is projected on the set of feasible velocities:

$$\frac{\mathrm{d}q}{\mathrm{d}t} = u = P_{C_q} \overline{U}. \tag{8}$$

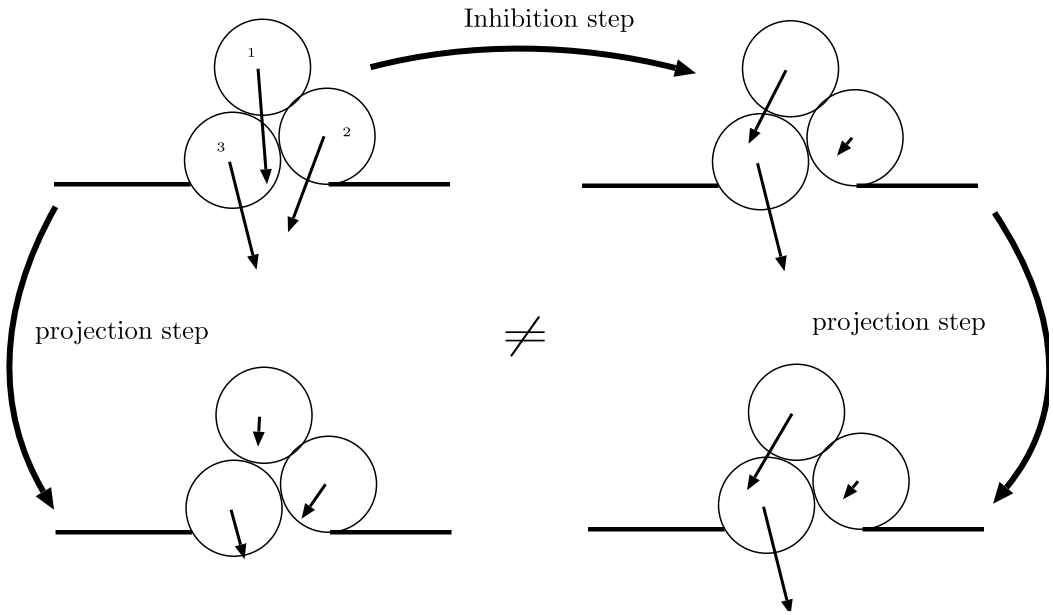

Figure 2: Plain granular model (straight projection on feasible velocities) and Inhibition Based version (inhibition step followed by a projection on feasible velocities).

The distinction with the plain granular model is illustrated in Figure 2: instead of straightly projecting the field of desired (purely selfish) velocities, we insert an intermediary step which implements the fact that each individual adapts their desired velocity to avoid pushing the people they see. In this simple 3-individual situation, the straight projection step leads to a drastic reduction of the speeds of 2 and 3, because they are in direct competition, and the least square projection builds the effective velocity field as a trade-off between all tendencies. In the case where desired velocities are inhibited (rightward arrow), individual 2 leaves priority to 3, which allows 3 to keep their desired velocity, whereas 2 drastically reduces their own. The final projection is here of no use, since all possible overlapping have been anticipated, and as a result the speed of 3 is much higher than the one which results from the straight projection. This simple example already illustrates the underlying mechanism of a Slower is Faster: by de-escalating some conflicts, the inhibition step allows people in front to progress faster.

The term *inhibited* has been used in this section to express the fact that it indeed corresponds to a tendency of some people to reduce their eagerness

to move forward. It deserves to be justified. It actually expresses the fact that the individual optimization procedure (6), that each individual performs, leads to a *decrease* of their velocity in the direction of their desired one. More precisely, if one assumes that all individuals that influence a given individual i lie in the half plane in front of i, i.e. if, for any i, all the $j \in V_i$ are such that $(q_j - q_i) \cdot U_i \geq 0$, then it can be straightforwardly established that

$$U_i \cdot \overline{U}_i \leq |U_i|^2, \tag{9}$$

or, equivalently, that $(\overline{U}_i - U_i) \cdot U_i \leq 0$. It means that the correction made on the desired velocity points downstream with respect to the desired direction U_i.

Remark 1. *(*Game theoretical approach*) This hierarchical model is a particular instance of a more general approach, based on the same principles, but without the acyclicity assumption. In this situation the problem consists in finding a collection of inhibited velocities* $\overline{U}_1, \ldots, \overline{U}_N$ *such that*

$$\overline{U}_i = \underset{w \in C_i(q, \overline{U}_{-i})}{\operatorname{argmin}} \frac{1}{2}|w - U_i|^2, \quad \forall i = 1, \ldots, N, \tag{10}$$

where

$$C_i(q, \overline{U}_{-i}) = \left\{ w \in \mathbb{R}^d,\ \forall j \in V_i,\ D_{ij}(q) = 0 \Rightarrow e_{ij}(q) \cdot (w - \overline{U}_j) \leq 0 \right\}. \tag{11}$$

We have used the standard convention in this game theoretic context: $\overline{U}_{-i}$ *denotes the collection of* $\overline{U}_j$*'s for* $j \neq i$*. This constitues the core of the approach : the feasible set for* i *depends on the strategies chosen by the other players. In case the graph contains cycles, the feasible set for* i *is likely to depend on the inhibited velocities of some* j*'s, the feasible set of which depend in return on* i*'s velocity. Any* $\overline{U}$ *solution to this problem can be considered as a Nash equilibrium for the game where pay-off functions depend on the distance to the individual desired velocities, and the strategy sets depend on the strategy of other players. The problem, which will be disregarded in this paper, has a different nature, and both existence and uniqueness of solution may be ruled out. We refer to Al Reda and Maury (2021) for a detailed account of mathematical issues raised by this approach.*

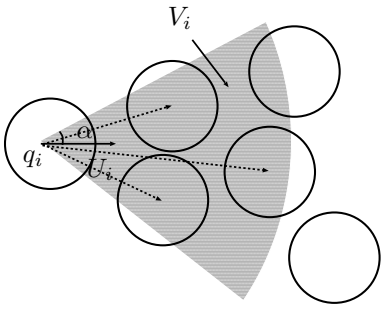

Figure 3: An example of a cone of vision and its corresponding influence graph

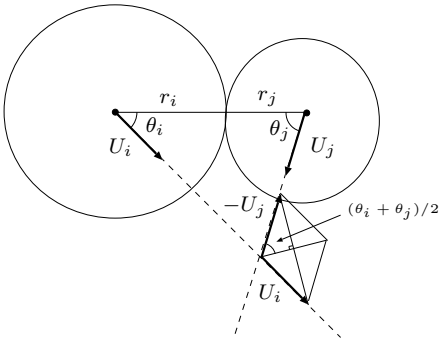

Figure 4: Notation

2.3. Hierarchy induced by the cones of vision

We consider here the case of an evacuation through a single exit door, and we assume that individuals are interchangeable, i.e. that the desired velocity of an individual depends on their position only. We denote by $U(\cdot)$ the common desired velocity field, so that $U_i = U(q_i)$. We furthermore consider that individuals are mainly influenced by others which they can see, i.e. that lie in their cones of vision. The cone of vision associated to i is defined as a conical zone centered at q_i and symmetric about the desired direction U_i (see Figure 3). It is fully determined by its half angle $\alpha > 0$, and by the range of vision (maximal distance below which individuals are accounted for). Yet, in our situation, this latter characteristic can be disregarded, because only individuals in contact are actually involved in the inhibition process, as stated in (7). Since the desired velocity field is not uniform but rather points to a given target, assuming $\alpha < \pi/2$ is not enough to rule out cycles.

Informally said, given an angle of vision α, the desired velocity field U

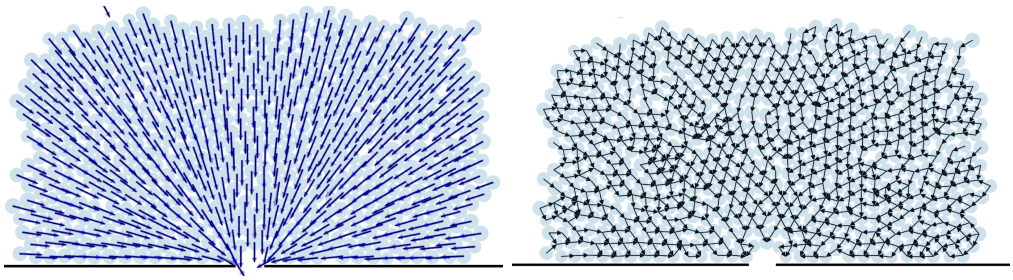

Figure 5: Desired velocities and associated influence graph

should not be too focusing to the point of creating mutually viewed individuals. Mathematically speaking, we ensure that two individuals i and j do not see each other mutually if $\max(\theta_{\mathrm{i}}, \theta_{\mathrm{j}}) > \alpha$, where $\theta_i = (\widehat{U_i, e_{ij}})$ and $\theta_j = (\widehat{U_j, e_{ji}})$ (see Figure (4)). To satisfy this constraint, it is sufficient to have

$$\cos\left(\frac{\theta_i + \theta_j}{2}\right) \leq \cos\alpha. \tag{12}$$

Moreover (see Figure 4), we have:

$$\cos\left(\frac{\theta_{\mathrm{i}} + \theta_{\mathrm{j}}}{2}\right) = \frac{||\mathrm{U_i} - \mathrm{U_j}||}{2} \leq \mathrm{r}\ ||\nabla \mathrm{U}||_2. \tag{13}$$

By prescribing the last term to be less than $\cos\alpha$, we obtain the following condition on the angle of vision α and the desired velocity U:

$$||\nabla U||_2 < \frac{\cos\alpha}{r}. \tag{14}$$

All the desired velocity fields used in the computations are based on the geodesic distance to a point that is located beyond the door (at a distance of 70 cm), to make people actually point outward the room. By making this choice, and by setting the angle of vision at a value that is not too wide ($\alpha = \pi/3$), we ensure that the dependence graphs do not contain cycles. Figure 5 represents the desired velocities together with the associated (oriented) influence graph for a crowd directed toward an exit.

3. Computational aspects

The numerical experiments presented in the next section are based on two models: the Granular Model (3) and the Inhibition Based model (6).

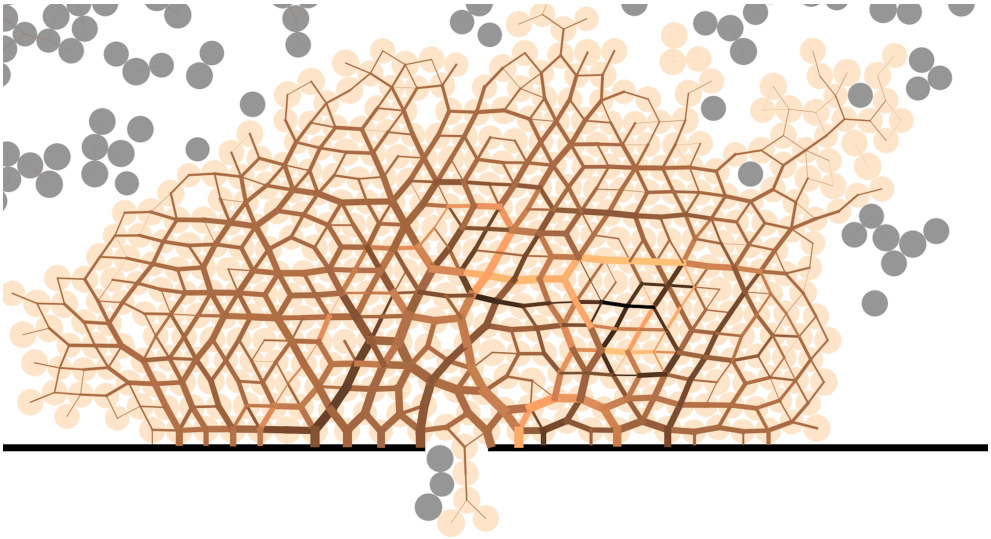

Figure 6: Granular evacuation. The width of an edge connecting disc centers is proportional to the interaction force between those discs.

As detailed in the previous section, the latter model is decomposed into two phases: first, inhibited velocities are computed in a frontal way (inhibition step). Then, once a preliminary field $\overline{U}$ has been built, it is projected on the set of feasible velocities (granular step).

3.1. Solving the granular model

The granular projection expressed by (3) amounts to project the desired velocity field U on C_q at any time. The time discretization procedure is inspired from a numerical scheme proposed in Maury (2006). We denote by $\tau > 0$ the time step, q^n the configuration at time $t^n = n\tau$. We also refer to Venel (2011) for Numerical Analysis issues concerning this approach. It relies on a first order expansion of the distances. Consider two grains i and j and associated velocities u_i and u_j. If they actually move with these velocities during a time $\tau > 0$, the new distance will be

$$D_{ij}(q^n + \tau u) \approx D_{ij}(q^n) + \tau e_{ij}(q^n) \cdot (u_j - u_i).$$

We accordingly introduce the discretized set of feasible velocities as

$$C^\tau(q^n) = \left\{ v \in \mathbb{R}^{2N},\ \forall j \neq i,\ D_{ij}(q^n) + \tau e_{ij}(q^n) \cdot (v_j - v_i) \geq 0 \right\}. \qquad (15)$$

A similar expansion will be used to define the discretized set of feasible velocities in the inhibition step, as detailed below.

The set $C^\tau(q^n)$ is a polyhedron with a number of face equal to the number of potential contacts, that is $N(N-1)/2$. In the context of regularly moving grain, most of these contacts can be ruled out: the constraints which are likely to be activated are limited to pairs of discs which are not too far away from each other, say at a distance of the order the size of the discs. Thus, the number of potentially active constraints grows linearly in N.

The saddle-point formulation of the minimization problem gives access to Lagrange multipliers that corresponds to contact forces. These contact forces pertain to pairs of discs in contact, they can be represented by modulating the width of edges of the contact graph, as illustrated by Figure 6. This saddle point formulation writes

$$\left|\begin{array}{lcl} u + B^\star p & = & U \\ Bu & \leq & b \\ p & \geq & 0 \\ \\ \langle p | Bu \rangle & = & 0. \end{array}\right. \tag{16}$$

where each row of B expresses a non-overlapping constraint, and $\langle \cdot | \cdot \rangle$ is the standard scalar product. This matrix is the discrete counterpart of the opposite of a divergence operator, and its adjoint $B^\star$ stands for a discrete gradient, making the problem stand as a discrete counterpart of a unilateral Darcy problem. Let us explain why this problem can be extremely ill-conditionned. Consider a situation where all constraints are saturated, i.e. $Bu \equiv 0$. Then p is the solution to a discrete Poisson problem

$$BB^\star p = BU + b.$$

The matrix $BB^\star$ is some sort of discrete Laplace operator, but it is highly degenerate. It can be checked in particular that its smallest eigenvalue can take arbitrarily small values.

Figure 6 represents a situation where the contact network is close to a triangular lattice. If it were perfectly structured, the kernel of $BB^\star$ would have a large dimension, and the matrix restricted to the orthogonal of this kernel would have a condition number close to that of a discrete Laplacian resulting from a Finite Difference discretization of the Laplacian in the two-dimensional setting, which is of the order N, that is the number of discs.

More precisely, for such a discrete Laplacian, the smallest eigenvalue is of order 1, and the largest eigenvalue scales like $1/h^2$, where h is the mesh step, which scales here like $1/\sqrt{N}$. In the granular setting, the network can be arbitrarily close to the triangular lattice, which creates arbitrarily small eigenvalues. As an illustration, the condition number of $BB^\star$ in the situation represented in Figure 6 is around 6×10^4, whereas the number of discs in the cluster is of the order 100.

3.2. Solving the inhibition-based model

At each time step, we start by re-indexing the individuals according to the topological sorting algorithm, so that any individual i is influenced by individuals with an index $j > i$. We keep the same notation for readability reasons. We update the individuals' positions as follows: $q^{n+1} = q^n + \tau u^{n+1}$ where u^{n+1} is the actual velocity computed in two steps, both based on a first order expansion of the non-overlapping constraint, like in the granular step.

The first step corresponds to individual adaptation (decision taking phase). We start with the highest index: individual N picks the velocity $\tilde{u}_N^n$ that approaches best their desired one U_N, subject to constraints with their neighbors. When i's turn comes, all velocities $\tilde{u}_{i+1}^n, \ldots, \tilde{u}_N^n$ have already been computed. For all $j \in V_i$ (set of individuals that lie in the cone of vision of i), if i takes the velocity w during τ, the first order expansion of D_{ij} writes

$$D_{ij}(q^n) + \tau e_{ij}(q^n) \cdot (\tilde{u}_j^n - w),$$

that is an affine expression which depends on velocities that have already been computed, thanks to the hierarchical ordering. We simply prescribe that the previous expression is non-negative, i.e. we prescribe

$$D_{ij}(q^n) + \tau e_{ij}(q^n) \cdot (\tilde{u}_j^n - \tilde{u}_i^n) \geq 0 \quad \forall j \in I_i.$$

The second step (global preservation of non-overlapping constraints) consists in projecting the adapted velocity $\tilde{u}^n$ on the set of admissible velocities that ensure the non-overlapping of individuals at each time step. These velocities should satisfy, for all $i \neq j$,

$$D_{ij}(q^n) + \tau e_{ij}(q^n) \cdot (u_j^n - u_i^n) \geq 0,$$

that is again the first order expansion of $D_{ij}(q^n + \tau u^n) \geq 0$.

To sum-up, the algorithm reads as follows:

1. (Inhibition step)
   We solve the following minimization problems in the following order $i = N, N-1, \dots, 1$:

$$\tilde{u}_i^{n+1} = \underset{w \in C_i^\tau(q^n, \tilde{u}_{-i}^n)}{\operatorname{argmin}} \frac{1}{2}|w - U_i(q_i^n)|^2$$

   where

$$C_i^\tau(q^n, \tilde{u}_{-i}^n) = \left\{ w \in \mathbb{R}^2,\ \forall j \in V_i(q^n),\ D_{ij}(q^n) + \tau e_{ij}(q^n) \cdot (\tilde{u}_j^n - w) \geq 0 \right\}.$$

   Note that, because of the hierarchical indexing, all indices j correspond to individuals that have already decided their velocity $\tilde{u}_j^n$.
2. (Projection step)
   The vector of inhibited velocities $\tilde{u}^{n+1}$ is projected on the set of globally admissible velocities (with respect to the non-overlapping constraint), like in the granular situation:

$$u^{n+1} = \underset{v \in C^\tau(q^n)}{\operatorname{argmin}} \frac{1}{2}|v - \tilde{u}^n|^2,$$

   where $C^\tau(q^n)$ is defined by(15).

Note that the minimization problems in the first step are local, they involve a very few degrees of freedom, and can be solved quasi-instantaneously. On the other hand, these problems have to be solved successively, which rules out any efficient parallelization strategy.

4. Comparison with experiments and paradoxical effects

We propose in this section to validate the Inhibition-based model with a hierarchy induced by cones of vision. We confront the numerical results of the model with some real evacuation experiments described in Garcimartín et al. (2014, 2016); Nicolas et al. (2017) to prove its ability to reproduce some phenomena. Also, a quantitative comparison is done between the numerical results of the Inhibition-Based model and the Granular Model Maury and Venel (2009, 2011) to highlight the difference between them concerning individuals' behavior.

Real evacuation experiments

We start by describing the real evacuation experiments involved in the comparison. The first set of experiments are evacuation drills done by Garcimartín et al. Garcimartín et al. (2014, 2016). During these experiments, a total of 85 participants are asked to exit a room through a door of width 75 cm. Two runs are done. In the first run, individuals are asked to exit the room as fast as they could while trying to avoid physical contact with others and pushing is banned (low competitiveness). In the second run, individuals are asked to do the same but they are allowed to push each other while evacuating (high competitiveness), excluding violent shoving. The main goal of these experiments is to test the evidence of the FIS effect experimentally. The presence of this effect was proved by showing that the evacuation time increases with the competitiveness level, and that the distribution of time lapses between consecutive egresses has a power-law tail, with a larger exponent for the low competitiveness case. Other controlled experiments are done in Nicolas et al. (2017) involving 80 participants asked to exit a room through a door of width 72 cm. For each run a fixed percentage of pedestrians are asked to behave selfishly, while the rest of individuals are asked to stay polite. The experiments are performed imposing "periodic boundary conditions" which means that evacuated pedestrians are re-injected in the room again after a while. A study of the correlations between time lapses is done in this paper as well as an analysis about their distribution and the dynamics in the exit zone. We refer the reader to Garcimartín et al. (2014, 2016); Nicolas et al. (2017) for more details about the experimental procedures.

Numerical simulations

We consider a square domain Ω with an exit door of width 75 cm located on one of the edges of the domain. We represent individuals by discs of diameters ranging between 35 cm and 40 cm considered as averages between the width and depth of a human body (see Weidmann (1993); Buchmueller and Weidmann (2006) for more details about parameters of pedestrians). We suppose that the desired velocity field U is the opposite of the normalized gradient of the distance to the exit door, i.e. $U(q) = -\nabla D(q)/|\nabla D(q)|$ where D is the distance to the exit door and q is the current configuration. The angle of the cones of vision is fixed to $\pi/3$, which guarantees an acyclic influence graph on the set of individuals (see Section 2.3).

We consider an initial configuration $q_0 \in K$ (defined by Equation (1)) of individuals randomly distributed on Ω and we set the time step at $\tau = 0.1$ s.

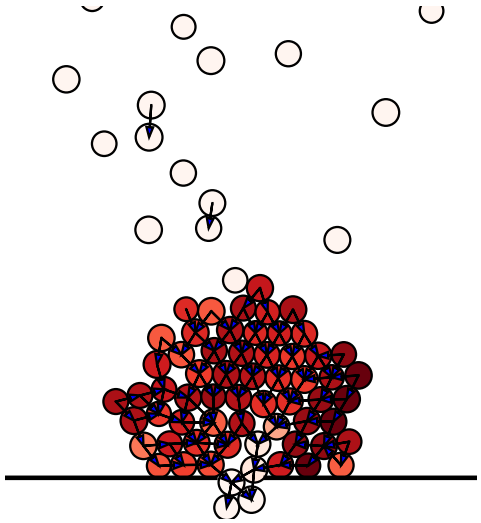

Figure 7: Snapshot of a periodic evacuation simulation using the Inhibition-Based model. Discs colors represent the frustration of individuals, which measures the deviation from their desired velocities (dark color when the frustration is high).

The motion is then computed according to the numerical scheme for the granular model (see Section 3.1), and for the IB model (see section 3.2).

The discs representing individuals have colors corresponding to their instantaneous frustration, as defined in Faure and Maury (2015):

$$f_i = 1 - (u_i \cdot U_i)/|U_i|^2$$

for each individual i. It is a dimensionless quantity, equal to 0 when the individual achieves their desired velocity and equal to 1 when the individual is not moving or has an actual velocity orthogonal to their desired one. The color of the discs ranges between white and dark red, white being for individuals going at their desired velocity and dark red for individuals not satisfied at all with their actual velocities. For the numerical simulations of the Inhibition-Based model, we sketch the influence graph based on the cones of vision for close individuals (see Figure 7). Figure 9 represents snapshots of an evacuation for the granular model, the IB model, and the IB model with an obstacle.

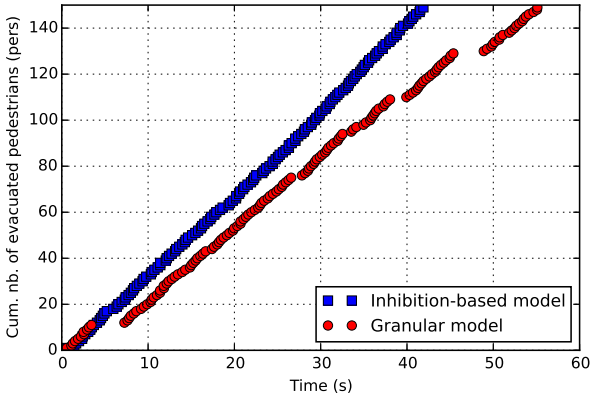

Figure 8: Cumulated number of evacuated pedestrians versus time for evacuation simulations using the granular model and the Inhibition-based model.

4.1. Faster is Slower

We aim at comparing two evacuation simulations for the Inhibition-based model and the granular model and find out whether these models are able to reproduce this effect. As mentioned in Subsection 1.3, individuals have a tendency to go slower in the direction where they want to go for the Inhibition-based model, compared to the granular model. Furthermore, using the saddle-point formulation of both models, one can show that the decision process based on the visual information of each pedestrian *reduces* their desired velocity in the desired direction of motion (see Inequality (9)).

We consider two evacuation simulations for the same initial configuration q_0 of $N = 150$ individuals using the granular model and the Inhibition-based model and extract all the time lapses between consecutive egresses. The door width is still 75 cm. Some snapshots of the evacuation simulations are represented in Figure 9 showing the occurrence of a jam upstream the exit door for the granular evacuation. To highlight the global difference, we represent in Figure 8 the cumulated number of evacuated individuals versus time that gives an overview of the evacuation process. The difference between the behavior of individuals is clear: the curve for the IB model is linear, while for the granular model there are some discontinuities caused by jams and the evacuation ends faster for the Inhibition-based model. Besides, the slope of each segment is smaller than the one associated to the Inhibition-Based model.

We compute empirically the mean of time lapses between consecutive

egresses and the flow mean for the granular model and the IB model. The result is displayed in Table 1. The mean flow is computed as the inverse of the mean of time lapses and the errors represent a 95 % confidence interval. The time lapses are smaller for the IB model compared with the granular one, and the flow undergoes an increase of 31.4 % which highlights the fact that individuals go globally faster for the IB model.

Model	Time lapses (mean)	Flow rate
Granular	0.41 ± 0.02 s	$2.42 \pm 0.1\,\mathrm{Ps}^{-1}$
Inhibition-Based	0.31 ± 0.004 s	$3.18 \pm 0.04\,\mathrm{Ps}^{-1}$
Inhibition-Based with obstacle	0.29 ± 0.003 s	$3.44 \pm 0.04\,\mathrm{Ps}^{-1}$

Table 1: Different evacuation situations with their respective mean of time lapses and flow rate.

4.2. Effect of an obstacle

As detailed in the introduction, the fluidizing effect of an obstacle can be seen as a particular instance of the FIS effect. In order to explore whether the Inhibition-Based model is able to reproduce this effect, we run two evacuation simulations for the same initial configuration (150 individuals, door width 75 cm) placing an obstacle upstream the door for one of them. The obstacle we consider here is a triangular obstacle placed 76.5 cm away from the exit door. Some snapshots of the simulations are shown in Figure 9 showing that the evacuation gets to its end faster in the case of the obstacle. The effect of an obstacle could also be observed for the periodic evacuation simulations when comparing the flow of pedestrians in two different cases: with and without an obstacle. The average flow of pedestrians is $3.18 \pm 0.04\,\mathrm{Ps}^{-1}$ for the simulation of the Inhibition-Based model without obstacle, versus $3.44 \pm 0.04\,\mathrm{Ps}^{-1}$ for the one with an obstacle upstream the door, so the average flow of pedestrians increases by 8.1%.

4.3. Alternation between short and long time lapses

This effect has been reported in Hoogendoorn et al. (2003); Hoogendoorn and Daamen (2005); Seyfried et al. (2009); Nicolas et al. (2017) and is known to occur when the width of the exit door is slightly less than two times the average size of a pedestrian. Actually, pedestrians tend to form lanes when evacuating that could be intercalated when the available space is low. In

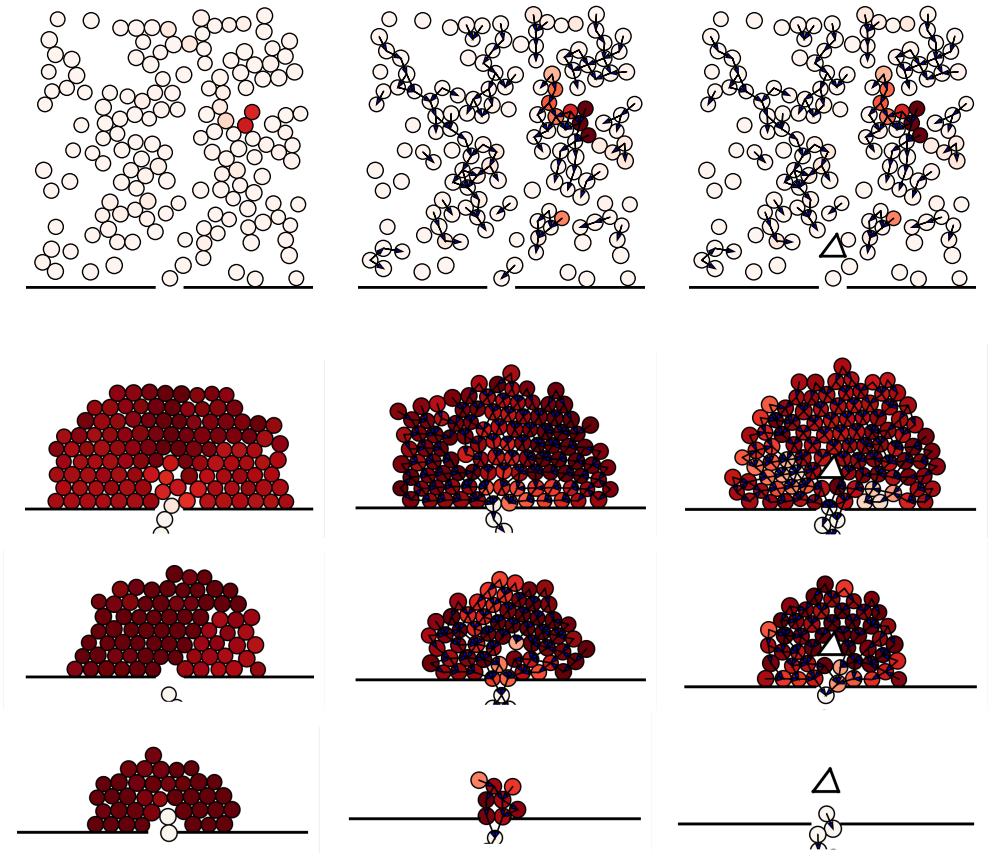

Figure 9: Evacuation of 150 pedestrians for: on the left, the granular model; on the middle the Inhibition-Based model; and on the right, the Inhibition-Based model with a triangular obstacle. The door width is 75 cm. Discs colors represent the frustration of individuals, which measures the deviation from their desired velocities (dark color when the frustration is high).

this case, individuals that are the closest to the exit door try to exit at the same time, but this is not possible due to the size of the exit. So what actually happens is that two pedestrians from neighboring lanes succeed to exit almost at the same time and then another pack of two pedestrians follows them. This effect was ascribed to a generalized zipper effect in Nicolas et al. (2017).

We aim to investigate whether the Inhibition-Based model is able to produce the alternation between short and long time lapses. For this purpose, we run an evacuation simulation for $N = 80$ individuals using the Inhibition-Based model where we impose "periodic boundary conditions" as for the experiments in Nicolas et al. (2017). The door width is 75 cm. Some seconds after the evacuation of an individual, we update his position and re-inject him in the room again at a random position (a snapshot of a periodic evacuation simulation is represented in Figure 7). We run the simulation during 3000 s and record all the exit times as well as the time lapses between two consecutive evacuations.

We compare the correlation function for numerical results with those of real data from the experiments described in Nicolas et al. (2017) and Garcimartín et al. (2014). The correlation function between time lapses Δt_i ordered by the rank of exit is defined by:

$$C(k) = \frac{\langle (\Delta t_i - \langle \Delta t \rangle)(\Delta t_{i+k} - \langle \Delta t \rangle) \rangle}{\langle (\Delta t_i - \langle \Delta t \rangle)^2 \rangle} \tag{17}$$

where the brackets denote an average over all pedestrians i in the experiment.

We plot in Figure 10 the correlation functions for the periodic evacuation experiment in Nicolas et al. (2017) (top), the non-periodic experiment with low competitiveness in Garcimartín et al. (2014) (middle), and the numerical simulation of the IB model with periodic boundary condition (bottom). The three plots show a negative dip for $k = 1$ meaning that statistically anti-correlation exists between successive time lapses, which asserts the effect for the real experiments, and the ability of the IB model to produce it for the numerical simulations. Moreover, the value of the correlation function for $k = 1$ is close to -0.2 for the numerical simulation and the low competitiveness experiment by Garcimartín et al. and is almost equal to -0.3 for the experiment by Nicolas at al.

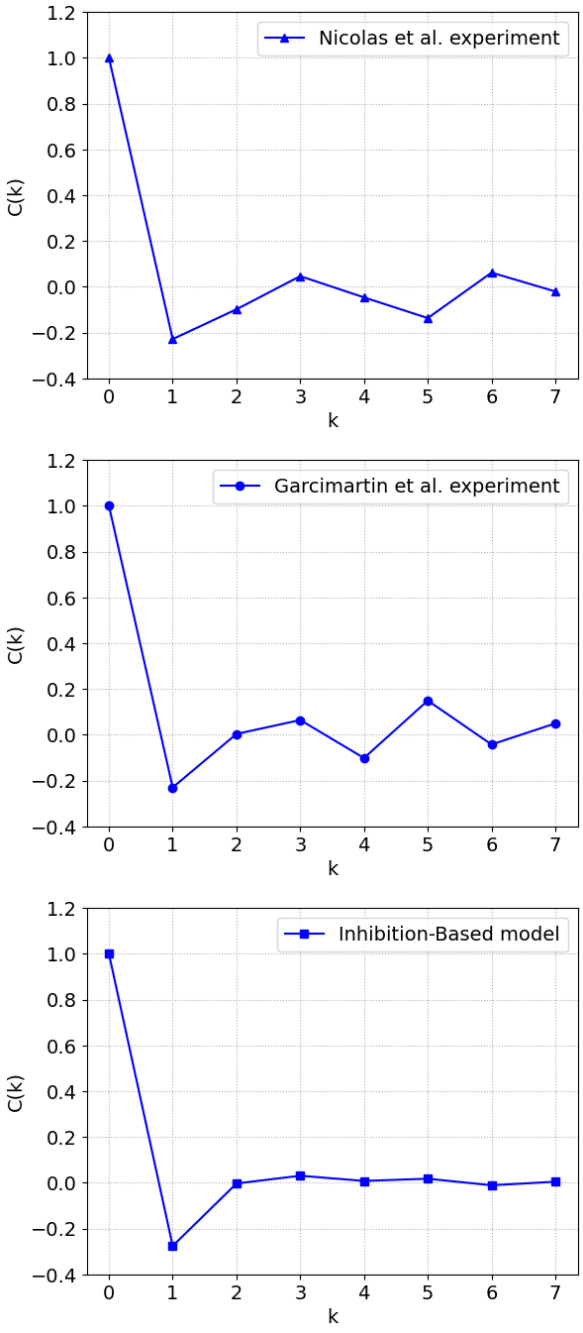

Figure 10: Correlation between time lapses for: periodic evacuation experiment by Nicolas et al. (2017) (top), evacuation experiment by Garcimartín et al. (2014) with low competitiveness (middle), and periodic evacuation simulation for the IB model (bottom).

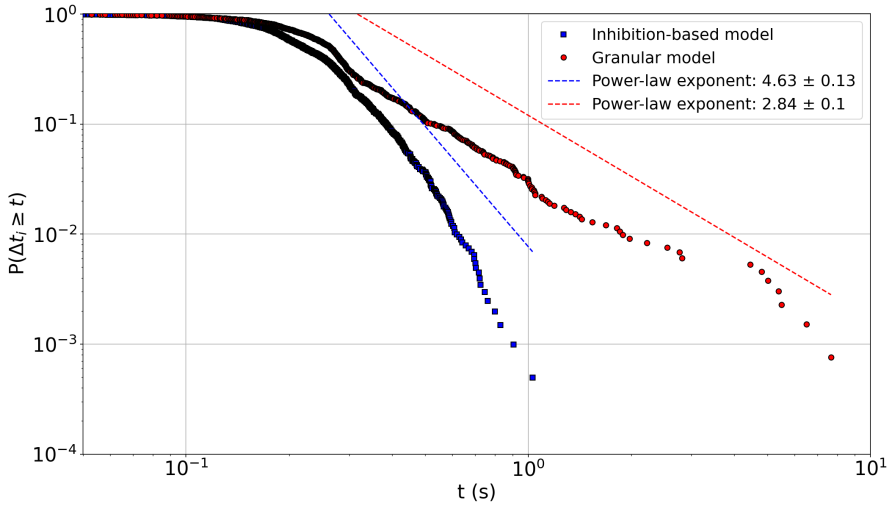

Figure 11: Complementary cumulative distribution functions for numerical simulations, granular model (red) and Inhibition-Based model (blue).

4.4. Power-law distribution of large time lapses

We are also interested in comparing the probability of occurrence of large time lapses between consecutive egresses for numerical simulations and real experiments.

For this purpose, we consider periodic evacuation simulations (as the ones described in Section 4.3) for both the granular model and the IB model and we extract all the time lapses between consecutive egresses. Then, we follow the procedure done in Garcimartín et al. (2014) where the authors plot the complementary cumulative distribution function (CCDF) for the two runs (low and high competitiveness), which is one minus the cumulative distribution function of time lapses. This probability distribution is computed as follows: we order the time lapses from smaller to larger, and for every time lapse Δt_k we empirically estimate the probability of finding a time lapse that is larger or equal to Δt_k. Note that a similar power-law distribution of time lapses has also been observed in suspensions of micro-swimmers forced to move through a micro exit (Al Alam et al. (2022)).

The CCDF for the periodic simulations is displayed in Figure 11 in a log-log scale. Using a dedicated tool to analyse such distributions (Python toolbox Powerlaw, see Clauset et al. (2009)), we fit the simulated distribu-

tion for the IB model with a power law, which gives an exponent 4.63 ± 0.13. This favorably compares to the 5.7 ± 0.8 obtained for the experiment with low competitiveness. Note that the fit with a power law is less obvious than for experimental data. Indeed, computed data can be fitted with an exponential law with a comparable accuracy: the log-likelihood ratio between both models is close to 0. For the granular model, the power law better matches the data, with an exponent of 2.84 ± 0.1 which is very low compared to the one obtained for the IB model (4.63 ± 0.13), and also compared to the experimental exponent (competitive egress), that is 5.0 ± 0.1. It means that long time lapses are more likely to occur in computations than experiments. This fact may be due to additional phenomena that appear in real life experiments to break jams whenever they occur, according to mechanisms that are not included in the model. Although the exponent for the granular model (2.84 ± 0.1) is not close to the one obtained for the high competitiveness case of the experiments (5.0 ± 0.1), and although the power law fit of the IB model is not perfect, these computations show that the time lapses for the IB model (low competitiveness) are much smaller that times lapses for the granular model (high competitiveness). Let us add that these considerations pertain to the distribution tail, which does not contain the mean value. These are nevertheless quite significant in terms of evacuation efficiency and safety since, as pointed out in Garcimartín et al. (2014), heavy tails express the occurence of large times lapses, which correspond to clogs, i.e. events where people are crushed upstream the exit.

4.5. Mixed behaviors and clogging

We investigate here the effect of different behaviors for the individual agents in the evacuation. In the spirit of the experimental setup detailed in Nicolas et al. (2017), we consider that individuals adopt one of two possible behaviors : a fixed fraction is considered panicked or selfish and moves according to the plain granular model, while the rest of the population is considered polite / inhibited, and is modeled by the IB model. The resulting algorithm is similar to the pure inhibition model: after the first hierarchical phase, the selfish individuals take their initial desired velocity before the last granular projection step is performed. We compare the influence of this mixed behavior on the probability of clogging and its effect on the flux. More precisely, we consider two situations:

1. Narrow door. Individuals are initially located randomly upstream the exit door, under conditions where clogs are likely to happen. For each

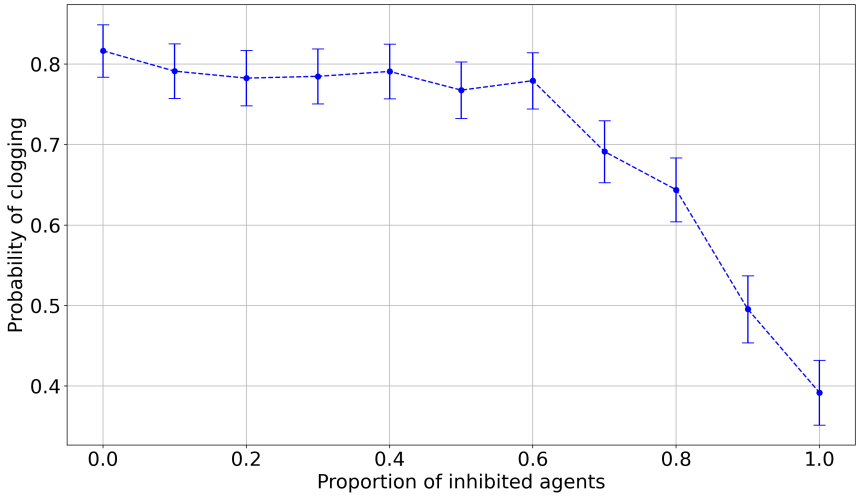

Figure 12: Probability of clogging vs. the proportion of inhibited agents. The number of agents is $N = 250$, and the door width is 75 cm.

proportion of inhibited agents, we perform a large number of simulations (600), and we estimate the clogging probability by counting the cases where a clog is still present after the final time 500 s, which is much larger than the evacuation time when everything goes fine (around 90 s). The results are presented in Figure 12

2. Large door. Individuals are initially located randomly upstream the exit door, under conditions (larger door) where clogs are **not** likely to happen. As previously, for each proportion of inhibited agents, we perform a large number of simulations (2000), and we estimate the mean evacuation time, averaged over the whole population, and also over the two subpopulations (inhibited and agressive).

In all scenarios, the number of individual is 250. Diameters randomly range over the interval [35 cm, 40 cm] (uniform distribution). In Case 1, the door width is 75 cm (narrow door), and in case 2, the door width is 135 cm (wide door).

Case 1 (narrow door): In Figure 12 we plot the estimated probability of stable clogs with respect to the proportion of inhibited agents. As mentioned previously, we consider that a stable clog occurs when there are still people

blocked upstream the exit when the computation ends. This figure exhibits a clear behavior: when the proportion of inhibited agents remains under a certain threshold value (around 60 %), there is no significant effect on the clogging probability, that remains around 0.8. But above this value, the clogging probability significantly decreases to the value of 0.4. This observation reproduces the fact that polite agents fluidizes the egress flow, in other words fewer conflicts make the evacuation faster, as observed in the experiments presented in Nicolas et al. (2017).

Case 2 (wide door): in this setting the door is sufficiently large to avoid clogs, all evacuations are completed in a finite time. Figure 13 plots the mean exit time with respect to the proportion of inhibited agents. The effect is less obvious and more subtle than in the first case. Indeed, for small proportions of inhibited people, the evacuation time is reduced. This reduction is small (around 7 %) but clearly visible on the plot. Yet, when this proportion is greater than 1/2, the effect is reversed: adding inhibited agent has a counterproductive effect on the evacuation (U-shaped curve). In other words, the left hand side of the plot expresses a Slower is Faster effect, whereas the right hand side corresponds to a non-paradoxical Faster is Faster. This series of simulations thus exhibits an optimal proportion of inhibited agents, that is around a half, in terms of evacuation efficiency. Note also that, even if inhibited people reduce the evacuation time for intermediate proportions, their own evacuation time is larger than the mean over all the population. In other words, they take benefit of their civilized behavior, but less that the agressive people, for whom the evacuation time is smaller.

4.6. Further exploration of the influence of an obstacle

We conclude this section by some additional tests to investigate the influence of the position of an obstacle upstream an exit door upon the evacuation process. We consider the experimental setting described in Feliciani et al. (2020): the door width is 75 cm, the number of evacuees is 180, and we considered the periodic setting: people are re-injected after they pass the door. The obstacle is a cylinder of diameter 40 cm, placed upstream the exit door at various distances. We investigated the distance range $[50\,\text{cm}, 250\,\text{cm}]$. We performed 300 evacuation simulations for each distance, with the granular model. For each of them, we simply count the number of passages during 500 seconds, and we compute its difference with the mean number without obstacle. Figure 14 represents, for each of the chosen distances, the mean relative number of passages, the $0.25 - 0.75$ percentile interval (rectangular

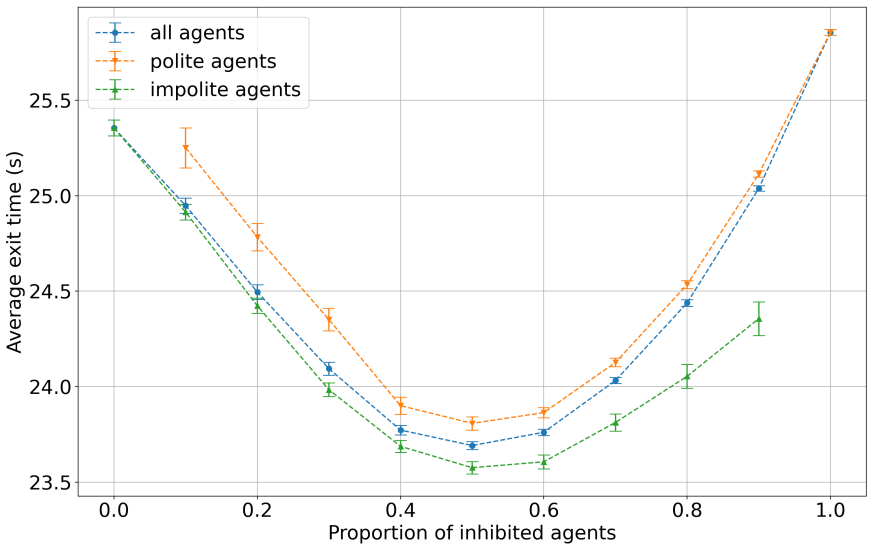

Figure 13: Average exit times vs. the proportion of inhibited agents, in situations where there was no clog. The average is performed over the whole population (blue), over polite agents only (orange), and over impolite agents only (green).

rectangle), the confidence interval and the fliers (extreme values represented as circles). The blue line corresponds to mean values for this relative number of passages. The distribution of passage numbers without obstacle is represented in the same graph, at the very left-hand side (distance 0), relative to the mean value, which is 75.

This series of results clearly exhibits the following behavior: two ranges of positions lead to a significant increase of the number of passages: around $d = 150$ cm and $d = 230$ cm. We added intermediate positions to assess whether they might correspond to artefacts, and the results for additional value in these neighborhood tend to confirm this tendency.

Figure 15 sheds light on the fluidizing role of the obstacle. We plotted the mean pressure (estimated as the Lagrange multiplier p of the non-overlapping constraint, see Eq. (16)) *relative* to the mean pressure computed in the case without obstacle, in 4 different situations. Blue indicates that the pressure is lower than in the situation with no obstacle, and red that it is higher. In all situations the red zone upstream the obstacle indicates higher pressure, as expected. For distances 100 cm and 175 cm (first and third plots), the red zone at the bottom indicates that congestion is increased upstream the door, in accordance to Figure 14, which indicates a decrease in evacuation efficiency. For distances 150 cm and 230 cm (second and fourth plots), the figure exhibits a blue zone right upstream the door, which indicates that congestion has been reduced, which is consistent with the fluidification of the evacuation expressed by Figure 14.

5. Conclusion

In this paper we studied the Faster-is-Slower effect from a granular modeling standpoint. We showed how a minimal parameter-free model based on individual inhibition reproduces effects which are similar to a series of laboratory experiments present in the literature.

The key ingredient of the model that we propose is the tendency of individuals to refrain from pushing the neighbors that lie in their cone of vision while other interactions are ruled out in a purely granular way. We show that turning on this tendency to avoid collisions with people upfront leads to an improvement of the global egress.

We investigated the ability of the model to reproduce the Faster is Slower effect by comparing some numerical simulations to real evacuation experiments present in the literature and find matching conclusions, up to the

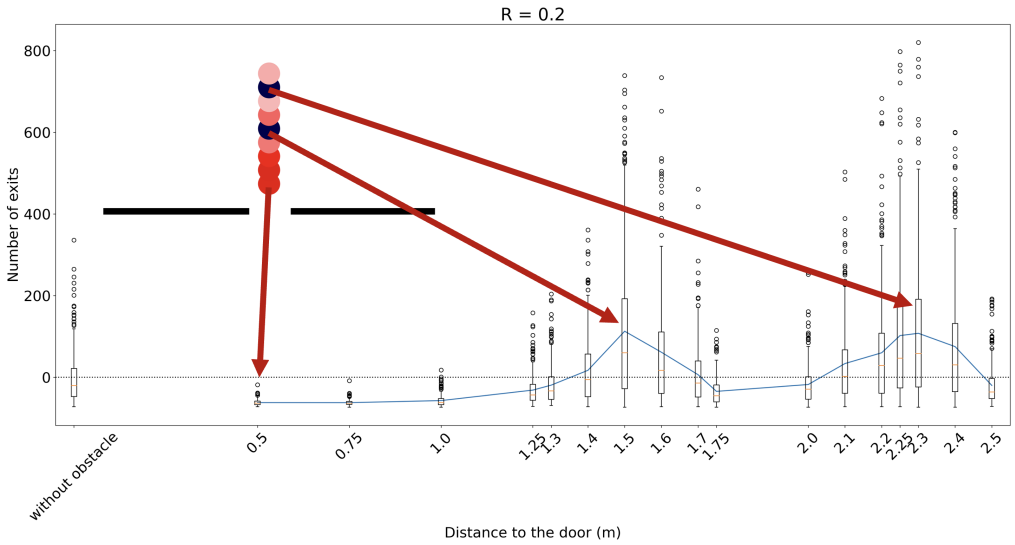

Figure 14: Variations of the number of exits with respect to door-obstacle distance. The coloured discs correspond to the various positions of the circular obstacle located upstream the exit. The values at the very left of the figure correspond to the situation without obstacle. The colors indicate the effect upon evacuation of the obstacle (compared to the case with no obstacle): red for a decrease of the number of exits, black for an increase of the number of exits (positive effect upon evacuation). These tests exhibit two distinct zones where the effect of the obstacle is *positive* upon evacuation efficiency (blue curve above the horizontal black line).

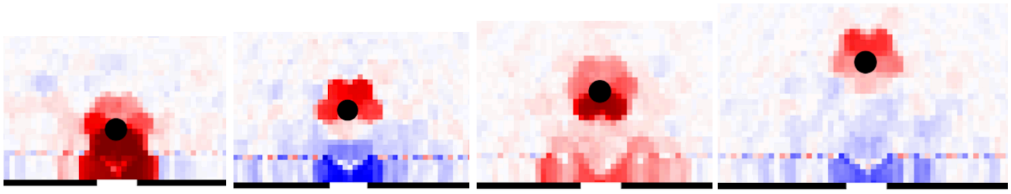

Figure 15: Mean pressure variations with respect to the no-obstacle situation, distances 1.0, 1.5, 1.75, 2.3

distribution of times lapses between consecutive egresses. We also validated the capacity of the model to reproduce other well known crowd motion phenomena like the fluidizing effect of an obstacle in some situations (see Shiwakoti et al. (2019) for a recent review on this controversial issue), and the alternation between short and long time lapses.

Finally, we studied the case where individuals adopt either a selfish or polite behavior, and found out that the probability to end up with a clogged simulation increases with the proportion of granular individuals.

The last point sets up a basis for a future work about the study of the effect of panic on evacuations: if we consider the purely asocial individuals as panicked, and the polite ones as calm, and consider a panic propagation model we could see what would happen if individuals have the ability to change from one state to the other in a continuous way. Another perspective is to consider evacuation scenarios with mutually interacting individuals, since the Inhibition-Based model strongly relies on a hierarchy of cones of vision. Indeed, if this hierarchy does not hold, the overall inhibition approach is ruled out, and it becomes necessary to set new rules to determine the actual velocities of mutually interacting agents, based on game theoretical ingredients.

Acknowledgments: The authors would like to thank A. Nicolas and A. Garcimartín for their precious help, and for providing experimental data.

References

Al Alam, E., Brun-Cosme-Bruny, M., Borne, V., Faure, S., Maury, B., Peyla, P., Rafaï, S., 2022. Active jamming of microswimmers at a bottleneck constriction. Phys. Rev. Fluids 7, L092301. URL: https://link.aps.org/doi/10.1103/PhysRevFluids.7.L092301, doi:10.1103/PhysRevFluids.7.L092301.

Al Reda, F., Maury, B., 2021. Game-theoretic and inhibition-based models for crowd motion. Comptes Rendus. Mathématique 359, 1071–1083.

Buchmueller, S., Weidmann, U., 2006. Parameters of pedestrians, pedestrian traffic and walking facilities. Institute for Transport Planning and Systems (IVT), Chair of Transport Systems, ETH Zurich.

Clauset, A., Shalizi, C.R., Newman, M.E.J., 2009. Power-law distributions in empirical data. SIAM Rev. 51, 661–703. URL: https://doi.org/10.1137/070710111, doi:10.1137/070710111.

Corbetta, A., Muntean, A., Vafayi, K., 2015. Parameter estimation of social forces in pedestrian dynamics models via a probabilistic method. Math. Biosci. Eng. 12, 337–356.

Cornes, F.E., Frank, G.A., Dorso, C.O., 2021. Microscopic dynamics of the evacuation phenomena in the context of the Social Force Model. Physica A: Statistical Mechanics and its Applications 568. doi:10.1016/j.physa.2021.125744, arXiv:2007.06746.

Daamen, W., Hoogendoorn, S.P., 2012. Emergency door capacity: Influence of door width, population composition and stress level. Fire Technology 48, 55–71.

Escobar, R., Rosa, A., 2003. Architectural design for the survival optimization of panicking fleeing victims, in: Lecture Notes in Computer Science. Springer. volume 2801, pp. 97 – 106.

Faure, S., Maury, B., 2015. Crowd motion from the granular standpoint. Mathematical Models and Methods in Applied Sciences 25, 463–493.

Feliciani, C., Zuriguel, I., Garcimartín, A., Maza, D., Nishinari, K., 2020. Systematic experimental investigation of the obstacle effect during non-competitive and extremely competitive evacuations. Scientific Reports 10, 15947. URL: https://doi.org/10.1038/s41598-020-72733-w, doi:10.1038/s41598-020-72733-w.

Garcimartín, A., Parisi, D., Pastor, J., Martín-Gómez, C., Zuriguel, I., 2016. Flow of pedestrians through narrow doors with different competitiveness. Journal of Statistical Mechanics: Theory and Experiment 2016, 043402.

Garcimartín, A., Zuriguel, I., Pastor, J., Martín-Gómez, C., Parisi, D., 2014. Experimental evidence of the "faster is slower" effect. Transportation Research Procedia 2, 760–767.

de Gennes, P., Brochard-Wyart, F., 2015. Gouttes, bulles, perles et ondes. Échelles, Humensis. URL: https://books.google.fr/books?id=DhSWDgAAQBAJ.

Gershenson, C., Helbing, D., 2015. When slower is faster. Complexity 21, 9–15. URL: https://onlinelibrary.wiley.com/doi/abs/10.1002/cplx.21736, doi:10.1002/cplx.21736.

Glowinski, R., Maury, B., 1997. Fluid-particle flow: a symmetric formulation. C. R. Acad. Sci. Paris 324, 1079–1084.

Haghani, M., 2020. Empirical methods in pedestrian, crowd and evacuation dynamics: Part II. Field methods and controversial topics. Safety Science 129, 104760. URL: https://doi.org/10.1016/j.ssci.2020.104760, doi:10.1016/j.ssci.2020.104760.

Helbing, D., Buzna, L., Johansson, A., Werner, T., 2005. Self-organized pedestrian crowd dynamics: Experiments, simulations, and design solutions. Transportation Science 39, 1–24.

Helbing, D., Farkas, I., Vicsek, T., 2000. Simulating dynamical features of escape panic. Nature 407, 487–490.

Hoogendoorn, S.P., Daamen, W., 2005. Pedestrian behavior at bottlenecks. Transportation science 39, 147–159.

Hoogendoorn, S.P., Daamen, W., Bovy, P.H., 2003. Extracting microscopic pedestrian characteristics from video data, in: Transportation Research Board Annual Meeting, pp. 1–15.

Jiang, L., Li, J., Shen, C., Yang, S., Han, Z., 2014. Obstacle optimization for panic flow-reducing the tangential momentum increases the escape speed. PloS one 9, e115463.

Kirchner, A., Nishinari, K., Schadschneider, A., 2003. Friction effects and clogging in a cellular automaton model for pedestrian dynamics. Physical review E 67, 056122.

Kirchner, A., Schadschneider, A., 2002. Simulation of evacuation processes using a bionics-inspired cellular automaton model for pedestrian dynamics. Physica A 312, 260–276.

Lakoba, T.I., Kaup, D.J., Finkelstein, N.M., 2005. Modifications of the helbing-molnár-farkas-vicsek social force model for pedestrian evolution. SIMULATION 81, 339–352. URL: https://doi.org/10.1177/0037549705052772, doi:10.1177/0037549705052772, arXiv:https://doi.org/10.1177/0037549705052772.

Lin, P., Ma, J., Liu, T., Ran, T., Si, Y., Wu, F., Wang, G., 2017. An experimental study of the impact of an obstacle on the escape efficiency by using mice under high competition. Physica A: Statistical Mechanics and its Applications 482.

Maury, B., 2006. A time-stepping scheme for inelastic collisions. Numerische Mathematik 102, 649–679.

Maury, B., Faure, S., 2018. Crowds in Equations: An Introduction to the Microscopic Modeling of Crowds. World Scientific.

Maury, B., Venel, J., 2009. Handling of contacts in crowd motion simulations. Traffic and Granular Flow'07 , 171–180.

Maury, B., Venel, J., 2011. A discrete contact model for crowd motion. ESAIM: Mathematical Modelling and Numerical Analysis 45, 145–168.

Moreau, J.J., 1977. Evolution problem associated with a moving convex set in a hilbert space. Journal of differential equations 26, 347–374.

Nicolas, A., Bouzat, S., Kuperman, M.N., 2017. Pedestrian flows through a narrow doorway: Effect of individual behaviours on the global flow and microscopic dynamics. Transportation Research Part B: Methodological 99, 30–43.

Parisi, D., Dorso, C., 2007. Why "faster is slower" in evacuation process, in: Pedestrian and Evacuation Dynamics 2005. Springer, pp. 341–346.

Pastor, J., Garcimartín, A., Gago, P.A., Peralta, J.P., Martín-Gómez, C., Ferrer, L., Maza, D., Parisi, D., Pugnaloni, L., Zuriguel, I., 2015. Experimental proof of faster-is-slower in systems of frictional particles flowing through constrictions. Phys. Rev. E 92.

Ruifeng Cao, J., Wai Ming Lee, E., Yuen, A.C.Y., Shi, M., Heng Yeoh, G., 2019. Slower is faster by considering of give-way evacuation behavior, in: 9th International Conference on Fire Science and Fire Protection Engineering (ICFSFPE), Chengdu, China, pp. 1–6.

Schadschneider, A., 2001. Cellular automaton approach to pedestrian dynamics-theory. arXiv preprint cond-mat/0112117 .

Schadschneider, A., Seyfried, A., 2009. Empirical results for pedestrian dynamics and their implications for cellular automata models, in: Pedestrian Behavior: Models, Data Collection and Applications. Emerald Group Publishing Limited, pp. 27–43.

Seyfried, A., Passon, O., Steffen, B., Boltes, M., Rupprecht, T., Klingsch, W., 2009. New insights into pedestrian flow through bottlenecks. Transportation Science 43, 395–406.

Shiwakoti, N., Shi, X., Ye, Z., 2019. A review on the performance of an obstacle near an exit on pedestrian crowd evacuation. Saf. Sci. 113, 54–67.

Sticco, I.M., Frank, G.A., Dorso, C.O., 2020. Effects of the body force on the pedestrian and the evacuation dynamics. Safety Science 129. doi:10.1016/j.ssci.2020.104829, arXiv:2003.02890.

Venel, J., 2011. A numerical scheme for a class of sweeping processes. Numerische Mathematik 118, 367–400. URL: https://doi.org/10.1007/s00211-010-0329-0, doi:10.1007/s00211-010-0329-0.

Weidmann, U., 1993. Transporttechnik der Fussgänger: Transporttechnische Eigenschaften des Fussgängerverkehrs (Literaturauswertung). ETH, IVT.

Xiaoping, Z., Wei, L., Chao, G., 2010. Simulation of evacuation processes in a square with a partition wall using a cellular automaton model for pedestrian dynamics. Physica A 389, 2177–2188.

Yanagisawa, D., A., K., Tomoeda, A., Nishi, R., Suma, Y., Ohtsuka, K., Nishinari, K., 2009. Introduction of frictional and turning function for pedestrian outflow with an obstacle. Phys Rev E Stat Nonlin Soft Matter Phys. 80.

Zuriguel, I., Olivares, J., Pastor, J.M., Martín-Gómez, C., Ferrer, L.M., Ramos, J.J., Garcimartín, A., 2016. Effect of obstacle position in the flow of sheep through a narrow door. Physical Review E 94, 032302.